Journal of Materials Chemistry A

Accepted Manuscript

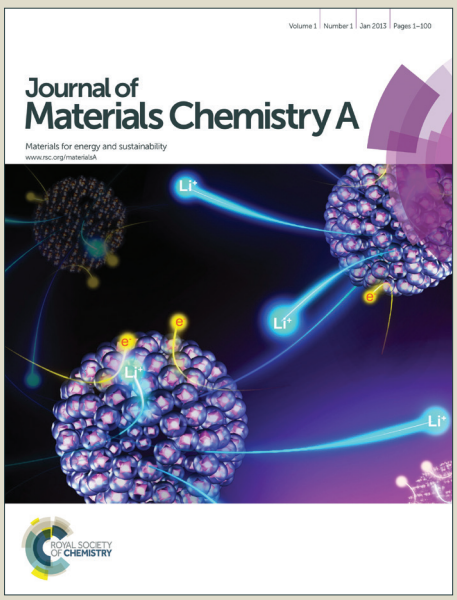

ROYAL SOCIETY OF CHEMISTRY

www.rsc.org/materialsA

Cite this: DOI: 10.1039/c0xx00000x

www.rsc.org/xxxxxx

ARTICLE TYPE

Sponge-like $NiCo_2O_4/MnO_2$ ultrathin nanoflakes for supercapacitor with high-rate performance and ultra-long cycle life

Gao Li,‡ Wenyao Li,‡ Kaibing Xu, Rujia Zou*, Zhigang Chen, Junqing Hu*

Received (in XXX, XXX) Xth XXXXXXXXX 20XX, Accepted Xth XXXXXXXXX 20XX

DOI: 10.1039/b000000x

We present a simple strategy for synthesizing sponge-like $NiCo_2O_4/MnO_2$ ultrathin nanoflakes which exhibit a high specific capacitance of 935 F g^{-1} at 1 A g^{-1}, excellent rate performance (74.9% retention at 50 A g^{-1}), and ultra-long cycling stability (103.1% of the initial capacitance after 25000 cycles).

Transition metal oxides (TMOs), especially in the form of nanomaterials, had been extensively studied as electrode materials of pseudocapacitors in the past decades.[1-5] This can be interpreted as their abundant Faradic redox reactions which contribute to high specific capacitances.[6] However, TMOs which redox reactions are involved often suffer from a lack of stability during long-term cycling.[7] Furthermore, the low electronic conductivity of TMOs profoundly restricts their rate performance.[8,9] An attractive concept to alleviate above negative effects is to combine two or more types of TMO nanostructures. Mixed TMOs as prospective electrode materials, which could inherit advantages from individual TMOs and generate excellent properties, have received an upsurge of interest in recent years. For instance, Xia *et al.*[10] reported Co_3O_4/NiO core-shell nanowire arrays for pseudocapacitors with an enhanced capacitance (853 F g^{-1} at 2 A g^{-1}), rate performance and electrochemical stability; Liu *et al.*[11] reported the MnO_2-NiO tube arrays for pseudocapacitors with an improved capacitance (0.35 F cm^{-2} at 8.5 mA cm^{-2}) with respect to pristine MnO_2 tubular arrays, a good cycle performance, and remarkable rate capability.

In addition to anticipating composition, the performance of TMOs in various applications also highly hinges on the microtexture of the materials.[12] Therefore, rational design of electrode materials with well-defined micro/nanostructures is imperative for further enhancement of the electrochemical properties. Hierarchical structures, which draw special interest due to their exceptional properties and remarkable potential in many fields, have been synthesized for many simple metal oxides, but the facile synthesis of the mixed TMOs with desirable composition and hierarchical structure still remains a challenge.[13, 14] So, it is desired that a well-designed compositions for supercapacitors with encouraging electrochemical performance, especially of high rate performance and long-time cycling stability, could be synthesized by a facile method.

Based on the above discussion, we present a simple strategy to fabricate sponge-like $NiCo_2O_4/MnO_2$ ultrathin nanoflakes on graphite paper with remarkable capacitive performance. $NiCo_2O_4$ and MnO_2 are composited into sponge-like ultrathin nanoflakes via a simple one-step electrodeposition with subsequent annealing. When applied as an electrode, the smartly designed composites possess three merits as follows: (I) ultrathin nanoflakes would enable a fast, reversible Faradaic reaction, and provide a short ion diffusion path, hence a good rate performance can be available;[15] (II) the fluffy sponge-like structure is advantageous to the permeation of the electrolyte to inner electrode as well as the emission of joule heat to the electrolyte, thus increasing the thermal stability of the structure;[16, 17] (III) ultrathin nanoflakes are strongly supported on graphite paper, in which binder and conductive additives can be avoided and consequently the 'inactive' surface is significantly reduced.[18] The electrochemical measurements show that the specific capacitance of the sponge-like $NiCo_2O_4/MnO_2$ ultrathin nanoflakes achieves a maximum of 935 F g^{-1} at a current density of 1 A g^{-1}, which could still retain 700 F g^{-1} (74.9% retention) even if the current density increase as high as 50 A g^{-1}. Moreover, the electrode maintains 103.1% capacitance of initialization after 25000 cycles, illustrating ultra-long cycling stability. These results show that the sponge-like $NiCo_2O_4/MnO_2$ ultrathin nanoflakes should be a very promising electrode material for supercapacitors.

Fig. 1a shows the X-ray diffraction (XRD) pattern of the $NiCo_2O_4/MnO_2$ ultrathin nanoflakes supported on graphite paper. As observed in Fig. 1a, except for the two strong peaks from the graphite paper substrate, other well-defined diffraction peaks confirm the existence of the spinel $NiCo_2O_4$ phase (JCPDS card no. 20-0781). The peak at 12.9° comes from the tetragonal MnO_2 phase (JCPDS card no. 44-0141). The chemical composition of the sample was further analyzed by X-ray photoelectron spectroscopy (XPS) shown in Fig. S1 (ESI†). High resolution XPS spectra of Mn 2p, Co 2p and Ni 2p for the $NiCo_2O_4/MnO_2$ ultrathin nanoflakes are presented in Fig. 1b-d. By using a Gaussian fitting method, Fig. 1b of Mn 2p region demonstrates two main peaks at 642.4 and 653.7 eV, indicating that the elemental Mn is in the formation of MnO_2.[11, 19, 20] The Co 2p spectrum (Fig. 1c) is best fitted considering two spin-orbit doublets characteristic of Co^{2+} and Co^{3+} and one shakeup satellites (identified as 'Sat.'). The Ni 2p spectrum (Fig. 1d) is best fitted considering two spin-orbit doublets characteristic of Ni^{2+} and Ni^{3+} and two shakeup satellites. These result show that the $NiCo_2O_4/MnO_2$ ultrathin nanoflakes has a composition containing Co^{2+}, Co^{3+}, Ni^{2+} and Ni^{3+}, which is in good agreement with literature for $NiCo_2O_4$.[18, 21] The uniform distribution of Mn,

Ni and Co species is also confirmed by the line-scan mapping (Fig. S2, see ESI†), which reveals that the composition is mainly composed of $NiCo_2O_4$ and only contains a few of MnO_2.

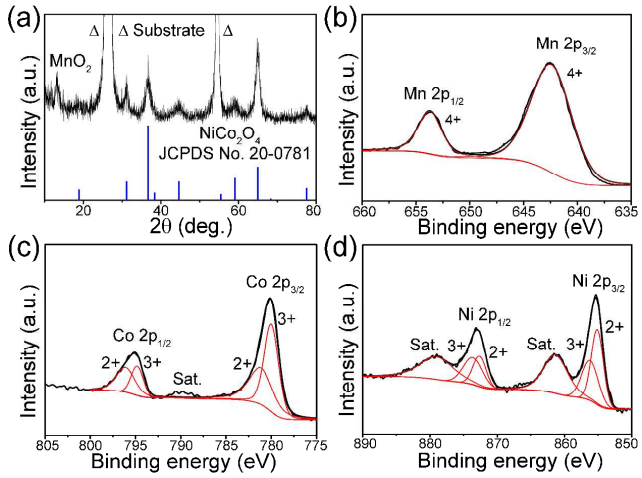

Fig. 1 (a) XRD pattern of the $NiCo_2O_4/MnO_2$ ultrathin nanoflakes. (b) Mn 2p, (c) Co 2p and (d) Ni 2p spectra of the $NiCo_2O_4/MnO_2$ ultrathin nanoflakes.

Low and high magnification field emission scanning electron microscopy (FESEM) images of the sample are shown in Fig. 2. A low FESEM image viewed from the top can be seen in the Fig. 2a, which indicates that the whole material on the graphite paper is homogeneous. High magnification image of the sample is shown in Fig. 2b, which reveals that the architecture is composed of numerous ultrathin nanoflakes (< 10 nm) and has a cross-linked character, in which channels and pores are formed. Low and high magnification FESEM images of the cross section are available in Fig. 2c, d, respectively. Fig. 2c reveals that the thickness of architecture is ~ 2 μm. Fig 2d elucidates that the ultrathin nanoflakes are standing over the graphite paper, thus it is beneficial to the charge transport and ion diffusion without the necessity of binder blocks, which results in better charge transfer kinetics. Notably, the cross-linked ultrathin nanoflakes provide a fluffy sponge-like architecture to facilitate the permeation of the electrolyte to inner electrode as well as the emission of joule heat to the electrolyte.

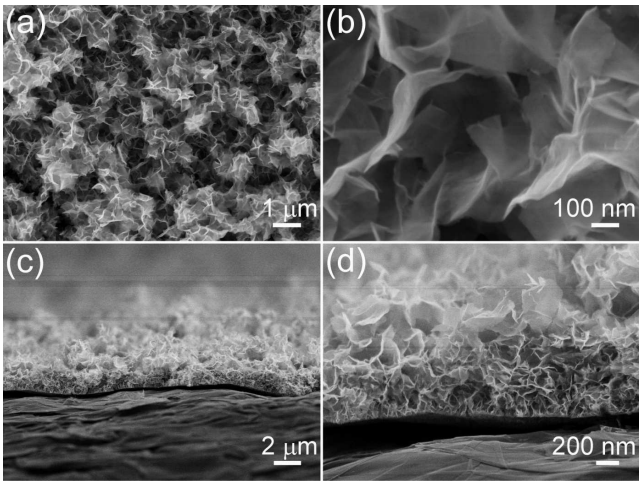

Fig. 2 (a) Low and (b) high magnification FESEM images from the top view, (c) low and (d) high magnification FESEM images of side view.

To better understand the structure, representative transmission electron microscopy (TEM) images taken from the sample are given in Fig. 3a, b. The dark strips in Fig. 3a are generally the folded edges or wrinkles of the nanoflakes. The magnified images of Fig. 3b clearly show that mesopores are uniformly distributed throughout the whole surface of nanoflakes. The size of the mesopores is estimated to be in the range of 2-5 nm. It is well known that the mesoporous structures in nanoflakes facilitate the mass transport of electrodes within electrolytes for Faradic redox reactions.[7, 22] The mesoporous structure will also enlarge the electrode/electrolyte contact areas, which further enhance the electrochemical performance of electrode.[12] As can be seen from the HRTEM image of Fig. 3c, the lattice fringes give an interplanar spacing of 0.23 nm and 0.20 nm, corresponding to that of the {222} and {400} lattice planes of the spinel $NiCo_2O_4$ crystal, respectively. EDX spectrum is shown in Fig. 3d. The presence of Mn, Co and Ni is in agreement with our designed concept, and the Cu and C signals clearly come from the TEM grid.

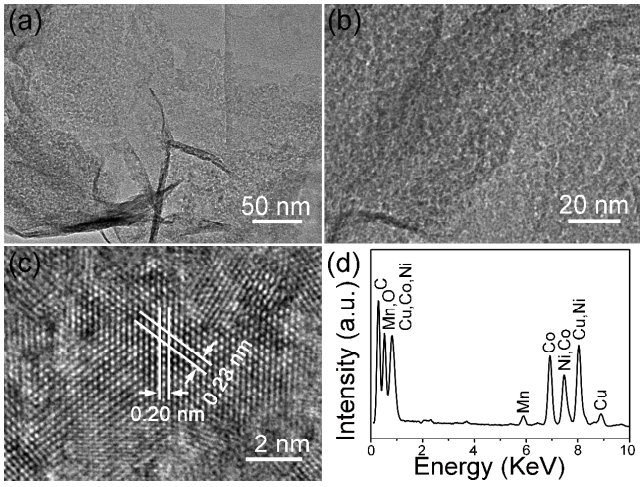

Fig. 3 (a) Low magnification TEM image. (b) Enlarged TEM image. (c) HRTEM image of $NiCo_2O_4/MnO_2$ ultrathin nanoflakes. (d) EDX pattern taken from ultrathin nanoflakes.

Electrochemical measurements were performed on an Autolab (PGSTAT302N) with a three-electrode configuration system in 1 M KOH aqueous solution within the potential window of -0.1 to 0.5 V (vs. Ag/AgCl) to evaluate the electrochemical performance of as-synthesized electrodes. The samples vary according to the electrodeposition time, namely 20, 30 and 40 min (denoted as P1, P2 and P3, respectively). The specific capacitance values of the samples had been determined by cyclic voltammetry (CV) and galvanostatic charge-discharge (CD) measurements. Fig. 4a shows the CV curves of the P1 sample at different scan rates. Strong redox peaks over the entire range of scan rates can be clearly observed, which reveals that the capacitive characteristics are mainly governed by Faradaic reaction. It is notable that the capacitance contributed from the graphite paper substrate is negligible (Fig. S3, ESI†).

It is well accepted that galvanostatic charge-discharge examination is an established method for estimating specific capacitance. Fig. 4b presents the typical charge-discharge voltage vs. time plots of the P1 sample at various current densities. A symmetric nonlinear triangular shape is observed, further

indicating their pseudo-capacitance behavior and excellent reversibility. The specific capacitance of the P1 sample at various current densities can be calculated based on the corresponding CD curves and the results are depicted in Fig. 4c together with the other two samples. The P1 sample manifests high specific capacitance values of 935, 923, 895, 863, 813, 770, 740 and 700 F g^{-1} at current densities of 1, 2, 5, 10, 20, 30, 40 and 50 A g^{-1}, respectively, which is superior to the other two samples (Table S1 in ESI†). This is mainly due to that as for the P2 and the P3 sample, a dense layer (Fig. S4, ESI†) covering on sponge-like ultrathin nanoflakes prevents the electrolyte from permeating into sponge-like ultrathin nanoflakes and only the outer surface of the dense layer can be utilized for the charge storage. It can be deduced that the thickness of the dense layer should increase as electrodeposition time goes on, and then specific capacitance values would decrease. The CD curves of the P2 and the P3 sample are shown in Fig. S5a, b (ESI†) for further demonstration. All of these samples simultaneously show high rate capability (74.9% for P1, 81.8% for P2, and 53.7% for P3) when current densities increase from 1 to 50 A g^{-1}, which can be ascribed to that ultrathin nanoflakes enable a fast Faradaic reaction and provide a short ion diffusion path.

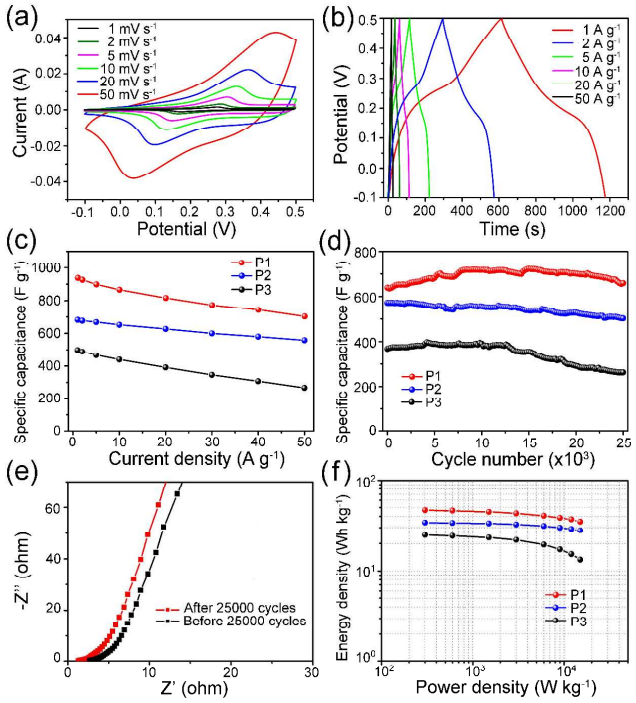

Fig. 4 (a) CV and (b) CD curves of the P1 sample. (c) Specific capacitance as a function of the current of P1, P2 and P3 samples. (d) Cycling performance of P1, P2 and P3 samples at a scan rate of 50 mV s^{-1}. (e) Nyquist plot of the P1 sample. (f) Ragone plots of P1, P2 and P3 samples.

Cycling stability is another critical factor in evaluating electrochemical properties of supercapacitor. The cycling stability curves of three electrodes at a scan rate of 50 mV s^{-1} are illustrated in Fig 4d. The final specific capacitance of the P1 sample retained 103.1% of its initial value when it had undergone 25000 cycles. In other words, the loss in specific capacitance based on the maximum value is only ~ 8.7%. Such an ultra-long cycle life can be ascribed to that the fluffy sponge-like structure is advantageous to the emission of joule heat to the electrolyte, hence increasing the thermal stability of the structure. However, cycling performances of the P2 (87.8% retention) and P3 (71.1% retention) samples are slightly satisfactory. It can be attributed to the denser layer of the P2 and P3 samples, which can't adapt well to the pronounced volume expansion/contraction and result the pulverization of electrode material. The Nyquist plots of the P1 sample are also presented in Fig. 4e. It is known that equivalent series resistance (ESR) is an important characteristic of supercapacitors measured at high frequency region where the curve intercepts on the real axis. The higher ESR indicates the lower electrical conductivity of the sample. It can be seen that the P1 sample shows ESR value ~ 2.7 Ω before cycling. After 25000 cycles, the P1 sample exhibits lower ESR (~ 1.3 Ω) which is due to the activation of active material during the cycling process. In addition, after 25000 cycles, the slope is close to 90° at low frequency region, which indicates that the P1 sample has good capacitive behaviour.

In view of excellent rate capability and ultra-long cycling life, we further calculate the energy and the power densities, which are the two key factors for the practical applications of supercapacitors. The results are presented as Ragone plots in Fig. 4f. The P1 sample can deliver high power output in the range of 0.3 and 15 kW kg^{-1} with little sacrifice of the high energy density (from 46.75 to 35 Wh kg^{-1}), better than that of the P2 (34.1 to 27.9 Wh kg^{-1}) and P3 (24.8 to 13.3 Wh kg^{-1}) samples. This result further confirms the sponge-like $NiCo_2O_4/MnO_2$ ultrathin nanoflakes of the P1 sample is an excellent capacitive material.

Based on above discussions, we have known that the sponge-like $NiCo_2O_4/MnO_2$ ultrathin nanoflakes of the P1 sample possessed the best electrochemical performance. However, it should be really understood whether this strategy to synthesize $NiCo_2O_4/MnO_2$ is of any advantage or not with respect to pure $NiCo_2O_4$, since $NiCo_2O_4$ exhibits a good pseudocapacitive behavior.[23-27] The pure $NiCo_2O_4$ was prepared by using the solution without $Mn(NO_3)_2$ in the same conditions. Electrochemical performances of the obtained pure $NiCo_2O_4$ and $NiCo_2O_4/MnO_2$ are shown in Fig. S6 (ESI†). Fig. S6a shows the cyclic voltammetry (CV) curves of $NiCo_2O_4/MnO_2$ and pure $NiCo_2O_4$ at a scan rate of 10 mV s^{-1}. The specific capacitance of pure $NiCo_2O_4$ is 1005 F g^{-1} which is higher than that of $NiCo_2O_4/MnO_2$ (839 F g^{-1}). Fig. S6b shows the galvanostatic charge-discharge (CD) curves of $NiCo_2O_4/MnO_2$ and pure $NiCo_2O_4$ at a current density of 5 A g^{-1}. The specific capacitance of pure $NiCo_2O_4$ is also larger than that of $NiCo_2O_4/MnO_2$. However, when we turn attention to rate performance and cycling stability of the materials, which are also important as specific capacitance, we find that $NiCo_2O_4/MnO_2$ acquired higher rate performance and much better cycling stability than pure $NiCo_2O_4$. Fig. S6c shows that $NiCo_2O_4/MnO_2$ exhibits higher rate performance of 74.9% retention compared with 70.3% retention from pure $NiCo_2O_4$. Fig. S6d indicates that $NiCo_2O_4/MnO_2$ possesses ultra-long cycling stability (103.1% of the initial capacitance after 25000 cycles), while pure NiCo2O4 can only retain 73.6% of its initial capacitance after 15000 cycles. Excellent rate performance and ultra-long cycling stability of $NiCo_2O_4/MnO_2$ demonstrate that this strategy is of advantage.

In summary, sponge-like $NiCo_2O_4/MnO_2$ ultrathin nanoflakes on graphite paper was synthesized by a simple process of electrodeposition with subsequent annealing. The as-synthesized electrode by 20 min electrodeposition exhibited an enhanced specific capacitance of 935 F g^{-1} at 1 A g^{-1} with high rate capability (74.9% capacity retention at 50 A g^{-1}) and ultra-long cycling stability (maintaining 103.1% capacitance of initialization after 25000 cycles). A high rate capability and ultra-long cycling stability make the sponge-like $NiCo_2O_4/MnO_2$ ultrathin nanoflakes to be a promising electrode material for high performance supercapacitors.

This work was financially supported by the NSFC (Nos. 21171035, 51302035 and 51272299), Key Grant Project of Chinese Ministry of Education (No. 313015), Ph.D. Programs Foundation of Ministry of Education of China (No. 20110075110008), Science and Technology Commission of Shanghai-based "Innovation Action Plan" (No. 10JC1400100), Fundamental Research Funds for the Central Universities, Shanghai Leading Academic Discipline (No. B603), Program of Introducing Talents of Discipline to Universities (No. 111-2-04).

Notes and references

[a] *State Key Laboratory for Modification of Chemical Fibers and Polymer Materials, College of Materials Science and Engineering, Donghua University, Shanghai 201620, China. Fax: +86-021-6779-2947; Tel: +86-021-6779-2947; E-mail: rjzou@dhu.edu.cn; hu.junqing@dhu.edu.cn*

† Electronic Supplementary Information (ESI) available. See DOI: 10.1039/b000000x/

‡ These authors contributed equally to the work.

1 W. Chen, R. B. Rakhi, L. B. Hu, X. Xie, Y. Cui, H. N. Alshareef, *Nano Lett.*, 2011, **11**, 5165.
2 C. Liu, F. Li, L. P. Ma and H. M. Cheng, *Adv. Mater.*, 2010, **22**, E28
3 C. Guan, J. Liu, C. Cheng, H. Li, X. Li, W. Zhou, H. Zhang and H. J. Fan, *Energy Environ. Sci.*, 2011, **4**, 4496.
4 R. B. Rakhi, W. Chen, D. Cha and H. N. Alshareef, *Nano Lett.*, 2012, **12**, 2559.
5 C. Yuan, L. Yang, L. Hou, L. Shen, X. Zhang and X. W. Lou, *Energy Environ. Sci.*, 2012, **5**, 7883.
6 J. Jiang, Y. Li, J. Liu, X. Huang, C. Yuan and X. W. Lou, *Adv. Mater.*, 2012, **24**, 5166.
7 P. Simon and Y. Gogotsi, *Nat. Mater.*, 2008, **7**, 845.
8 C. C. Hu, K. H. Chang, M. C. Lin and Y. T. Wu, *Nano Lett.*, 2006, **6**, 2690
9 Y. B. He, G. R. Li, Z. L. Wang, C. Y. Su and Y. X. Tong, *Energy Environ. Sci.*, 2011, **6**, 5531.
10 X. H. Xia, J. P. Tu, Y. Q. Zhang, X. L. Wang, C. D. Gu, X. B. Zhao and H. J. Fan, *ACS NANO*, 2013, **6**, 5531.
11 J. P. Liu, J. Jiang, M. Bosman, H. J. Fan, *J. Mater. Chem. A*, 2012, **22**, 2419
12 H. B. Wu, H. Pang and X. W. Lou, *Energy Environ. Sci.*, 2013,**6**, 3619.
13 L. Xiao, Y. Yang, J. Yin, Q. Li and L. Zhang, *J. Power Sources*, 2009, **194**, 1089.
14 Q. Wang, B. Liu, X. Wang, S. Ran, L. Wang, D. Chen and G. Shen, *J. Mater. Chem.*, 2012, 22, 21647.
15 L. Yu, G. Q. Zhang, C. Z. Yuan, X. W. Lou, Chem. Comm., 2013, 49, 137.
16 J. Yan, W. Sun, T. Wei, Q. Zhang, Z. Fan and F. Wei, *J. Mater. Chem.*, 2012, 22, 11494.
17 C.Y. Cao, W. Guo, Z.M. Cui, W.G. Song and W. Cai, *J. Mater. Chem.*, 2011, 21, 3204.
18 C. Z. Yuan, J. Y. Li, L.R. Hou, X. G. Zhang, L. F. Shen,X. W. Lou, *Adv. Funct. Mater.,* 2012, 22, 4592
19 H. W. Nesbitt, D. B. Anerjee, *American Mineralogist,* 1998, 83, 305
20 C. Zhou, H. Wang, F. Peng, J. Liang, H. Yu, J. Yang, *Langmuir* 2009, 25, 7711.
21 B. Cui, H. Lin,Y. Z. Liu, J. B. Li, P. Sun, X. C. Zhao, C. J. Liu, *J. Phys. Chem. C*, 2009, 113, 14083.
22 Z. Wang, L. Zhou, X. W. Lou, *Adv. Mater.*, 2012, 24, 1903.
23 L. F. Shen, Q. Che, H. S. Li, X. G. Zhang, *Adv. Funct. Mater.*, DOI: 10.1002/adfm.201303138.
24 G. Q. Zhang, H. B. Wu, H. E. Hoster, M. B. Chan-Park, X. W. Lou, *Energy Environ. Sci.*, 2012, 5, 9453.
25 G. Q. Zhang, X. W. Lou, *Adv. Mater.*, 2013, 25, 976.
26 W. L. Yang, Z. Gao, J. Ma, X. M. Zhang, J. Wang, J. Y. Liu, *J. Mater. Chem. A*, 2014, 2, 1448.
27 C. Z. Yuan, J. Y. Li, L. R. Hou, J. D. Lin, X. G. Zhang, S. L. Xiong, *J. Mater. Chem. A*, 2013, 1, 11145.